Transparent lithium-ion batteries

Yuan Yang[a], Sangmoo Jeong[b], Liangbing Hu[a], Hui Wu[a], Seok Woo Lee[a], and Yi Cui[a,1]

[a]Departments of Materials Science and Engineering and [b]Electrical Engineering, Stanford University, Stanford, CA 94305

Edited* by Tobin J. Marks, Northwestern University, Evanston, IL, and approved June 20, 2011 (received for review February 20, 2011)

Transparent devices have recently attracted substantial attention. Various applications have been demonstrated, including displays, touch screens, and solar cells; however, transparent batteries, a key component in fully integrated transparent devices, have not yet been reported. As battery electrode materials are not transparent and have to be thick enough to store energy, the traditional approach of using thin films for transparent devices is not suitable. Here we demonstrate a grid-structured electrode to solve this dilemma, which is fabricated by a microfluidics-assisted method. The feature dimension in the electrode is below the resolution limit of human eyes, and, thus, the electrode appears transparent. Moreover, by aligning multiple electrodes together, the amount of energy stored increases readily without sacrificing the transparency. This results in a battery with energy density of 10 Wh/L at a transparency of 60%. The device is also flexible, further broadening their potential applications. The transparent device configuration also allows in situ Raman study of fundamental electrochemical reactions in batteries.

energy storage | flexible electronics | self-assembly | transparent electronics

Transparent electronics is an emerging and promising technology for the next generation of optoelectronic devices. Transparent devices have been fabricated for various applications, including transistors (1–6), optical circuits (7), displays (8–10), touch screens (11), and solar cells (12–14). However, the battery, a key component in portable electronics, has not been demonstrated as a transparent device. Consequently, fully integrated and transparent devices cannot be realized because the battery occupies a considerable footprint area and volume in these devices (e.g., cell phones and tablet computers). Typically, a battery is composed of electrode materials, current collectors, electrolyte, separators, and packaging (15). None of them are transparent except for the electrolyte. Furthermore, as these components are in series, all of them must be clear to make the whole device transparent. A widely used method for making transparent devices is to reduce the thickness of active materials down to much less than their optical absorption length, as demonstrated in carbon nanotubes (5, 7), graphene (11), and organic semiconductors (12, 14). However, this approach is not suitable for batteries, because, to our knowledge, no battery material has an absorption length long enough in the full voltage window. For example, $LiCoO_2$ and graphite, the most common cathode and anode in Li-ion batteries, are good absorbers even with a thickness less than 1 μm. Moreover, black conductive carbon additive is always required in electrodes, which occupies at least 10% of the total volume (16). In contrast, to power common portable electronics, the total thickness of electrode material needs to be on the order of 100 μm–1 mm, much longer than the absorption length of electrode materials. This dilemma comes from the fact that the transparency of materials decays exponentially with the thickness, whereas the amount of energy stored increases only linearly with the thickness. Some transparent materials, such as indium oxide (In_2O_3), could be used as battery materials. However, upon cycling, metal nanoparticles and lithium oxides are formed, significantly deteriorating the transparency (Figs. S1 and S2) (17). To overcome these challenges, we demonstrate a unique microfluidics-assisted method to make a patterned grid-like battery electrode filled with nanomaterials. The battery appears transparent as the patterned electrode materials cover only a small portion of the whole area and the pattern features are smaller than the detection limit of human eyes. Li-ion batteries with different transparencies were fabricated. For example, a full cell with an energy density of 10 Wh/L, including packaging, is demonstrated at a transparency of 60%. Furthermore, by aligning multiple transparent batteries in series, the energy stored could scale up easily without sacrificing the transparency of the device. Finally, we show that such a device is also a powerful tool for in situ optical studies of electrochemical reactions in batteries.

Results

Design and Fabrication of Transparent Li-Ion Batteries. To circumvent the intrinsic problem of the opacity of battery electrode materials, we utilize a previously undescribed strategy of designing patterned electrodes with very small features so that the nontransparent materials cover only a small portion of the whole area of the device, as illustrated in Fig. 1*A*. The opaque battery electrode materials (black) and metal current collectors (yellow) beneath are confined inside the grid, whereas the rest of the electrode substrate is transparent. If the feature dimension of the lines is comparable or less than the resolution of human eyes (50–100 μm), the opaque electrode grid is indistinguishable from the transparent substrate. Consequently, the entire device appears transparent. At a transparency of α, the areal portion of opaque electrode materials is $1 - \alpha$. Moreover, by aligning multiple layers of electrodes together, the transparency does not decrease, whereas the energy stored increases linearly. In contrast, the transparency of thin film electrodes decreases exponentially when more cells are stacked in series (18, 19). As a result, a transparent battery with practical capacity for portable electronics can be accomplished using patterned electrodes on clear substrates. Fig. 1*B* plots the calculated transparency versus volumetric energy density of such devices. The theoretical limit based on only active materials is shown in black, whereas the red line considers the volume of all other components in a battery, including current collectors, separators, and packaging. At a transparency of 60%, the theoretical energy density is about 100 Wh/L with packaging, which is comparable to the energy density of lead acid and NiCd rechargeable batteries (see *SI Text*) (15). By varying the width and space in the grid, we fabricate batteries with transparency of 30%, 60%, and 78%, as indicated by the green triangles in Fig. 1*B*. The corresponding energy density is 20, 10, and 5 Wh/L considering packaging, which proves the feasibility of this approach.

The concept of patterned electrodes is an effective method to fabricate transparent batteries. However, realizing such a structure is not trivial, especially for batteries. The battery electrode is a thick porous film (typically 30–300 μm), composed of heterogeneous powders with entirely different properties: inorganic

Author contributions: Y.Y. and Y.C. designed research; Y.Y., S.J., L.H., and H.W. performed research; Y.Y., S.J., L.H., and S.W.L. analyzed data; and Y.Y. and Y.C. wrote the paper.

The authors declare no conflict of interest.

*This Direct Submission article had a prearranged editor.

Freely available online through the PNAS open access option.

[1]To whom correspondence should be addressed. E-mail: yicui@stanford.edu.

This article contains supporting information online at www.pnas.org/lookup/suppl/doi:10.1073/pnas.1102873108/-/DCSupplemental.

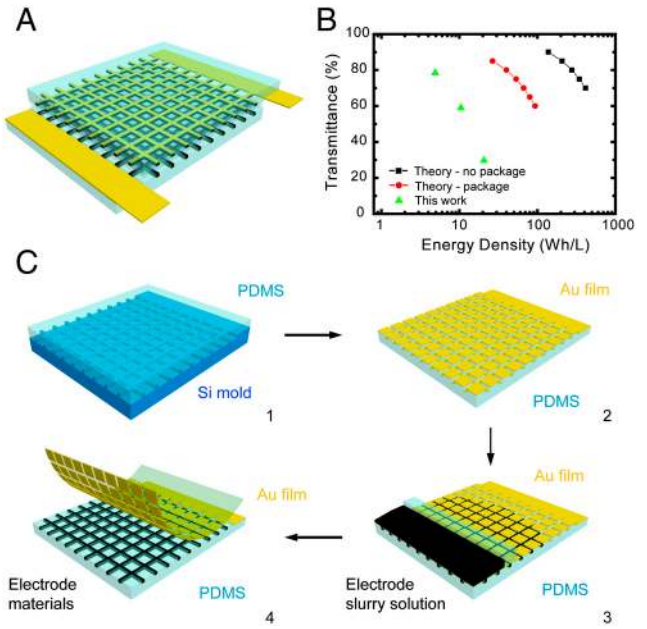

Fig. 1. (*A*) The schematic of a transparent battery with grid-like patterned electrodes. In contrast to using thin film electrodes, this concept allows scalable energy storage while maintaining high transparency. The different colors indicate the PDMS substrate (light blue), electrode materials (black), and metal current collector (yellow). (*B*) The transparency versus volumetric energy density. The black line is only active materials and the red line considers the volume of other components, such as separators, current collectors, and packaging. (*C*) The process flow of fabricating a transparent battery: (1) Transfer grid patterns from silicon mold to PDMS, (2) evaporate gold current collector onto the PDMS substrate, (3) fill in battery electrode materials by a microfluidics-assisted method, and (4) peel off gold film on top of the PDMS substrate.

active materials, carbon black nanoparticles, and an adhesive organic binder. Moreover, the electrochemical performance of these materials is sensitive to damage (20) and surface modifications (21). Hence, traditional etching or lithography methods used in electronics processing are not appropriate. Ink-jet printing, which requires low-viscosity inks, is an effective approach to make thin patterned electrodes. However, it is difficult to transfer enough solid mass and print very narrow lines with low-viscosity inks. Moreover, materials patterned by ink-jet printing without confinement are likely to crack and diffuse away from their initial position, which could significantly decrease the transparency during long-term operation. To overcome these difficulties, we demonstrate a unique microfluidics-assisted method to pattern battery materials (Fig. 1*C*). This approach is related to microchannel guided assembly of nanomaterials (22, 23), but uses a distinct configuration. First, a polydimethylsiloxane (PDMS) substrate with grid-like trenches is fabricated by spin coating a PDMS precursor onto a silicon mold and curing it at 80 °C for 3 h. The width of the trenches is 35 μm. After the PDMS is peeled off from the silicon mold, a 100-nm gold film is evaporated onto it as the current collector. Then, the sample is treated in air plasma for 90 s to make its surface hydrophilic. A thin slide of PDMS, referred to as the blocking PDMS in step 3, is placed at one end of the trenches to form a narrow region of closed channels (2–3 mm in length). After an aqueous slurry solution containing the active electrode material (18–20 wt % in water) is dropped onto one side of the blocking PDMS, capillary forces pull it into the closed channels, from which it continues to flow through all of the trenches in the device (Fig. 1*C*). The flow speed is about 1 cm/s. We find that nano-sized active materials filled the trenches more quickly and evenly than micron-sized particles. This is likely because nanomaterials do not clog the channels easily, even when the slurry solution is concentrated. As a result, $LiMn_2O_4$ nanorods (20, 24) and $Li_4Ti_5O_{12}$ nanopowder are used as cathode and anode materials, respectively. An analytical model on the estimate of the flow speed is made based on simple closed round channels. The filling length L is equal to $(\frac{R\gamma\cos\theta}{2\mu})^{1/2}t^{1/2}$, where R is the radius of channel, γ is the surface tension of water, θ is the contact angle, μ is the viscosity of the slurry solution, and t is time. The time to fill a 1-cm channel will take only 0.4 s, which is consistent with observations (see *SI Text* for more details). The filling speed can be further increased by lowering the viscosity of the solution. This filling rate has the same order of magnitude as the rate of a conventional coating method for battery electrodes, suggesting its compatibility with large-scale production. After drying and removing the blocking PDMS, all of the trenches are filled with battery electrode material. The next step is to peel off the extra gold on top of the PDMS with Kapton tape. The gold film is readily removed due to a low surface energy of PDMS (19.8 J/m^2) (25). This process results in the fabrication of a single transparent electrode with both metal current collectors and electrode materials confined in microtrenches. Then the two electrodes and a piece of transparent gel electrolyte are assembled together; this is another key step in this grid-based design. If the grid patterns in the two electrodes do not match well to each other, the transparency will decrease exponentially upon stacking, as in the case of thin film electrodes. Cell assembly is performed manually under optical microscopy at a magnification of approximately 20×, which results in an accuracy better than 10 μm. This assembly process can be done automatically in the future in real battery production with better aligning accuracy. Finally, the sandwich structure is sealed inside a transparent polymer bag with two pieces of aluminum strip extending out as the current collector, which has the same configuration as pouch cell, except that all components are transparent.

Microscopic Characterizations of Components in Transparent Batteries. Fig. 2 *A–C* shows a series of images of an as-fabricated single transparent electrode on a polyethylene naphthalate substrate at different magnifications. The areal portion of trenches is 35%, indicating a theoretical transparency of 65%. Characters behind the electrode can be seen clearly in the camera image (Fig. 2*A*). The electrode is also bendable and flexible. High magnification optical images (Fig. 2*B*) and the SEM image (Fig. 2*C*) illustrate that the electrode materials are confined to the interior of the trenches, demonstrating that the microfluidics-assisted method is successful in patterning battery electrodes. An optical microscope is used to study the uniformity and thickness of battery electrode materials inside the trenches. The average thickness is 50 μm, which is about 70% of the trench depth and comparable with the thickness of electrode materials in commercial batteries. Moreover, this portion is much higher than the concentration of solid material in the slurry (18–20%), suggesting that the solution keeps moving toward the end of trenches upon evaporation of water. The standard deviation of the thickness is 4 μm, corresponding to a small variation of 8% over the whole device (Fig. S3). This indicates that the microfluidics-assisted method forms a uniform electrode film and the mass loading is suitable for practical use. Along with the electrodes, a separator between the cathode and the anode is necessary to avoid internal shorting. However, common separators made of polypropylene and polyethylene are opaque (26). Therefore, a transparent gel electrolyte, which also acts as a separator, is used to solve this problem. In this study, a gel electrolyte of poly(vinylidene fluoride-co-hexafluoropropylene) (PVDF-HFP) membrane permeated with 1 M $LiClO_4$ in ethylene carbonate/diethyl carbonate (EC/DEC) is developed. The gel membrane is elastic and highly transparent, as illustrated in Fig. 2*D*.

As mentioned before, the grid structure in electrodes must align with each other to achieve high transparency and high en-

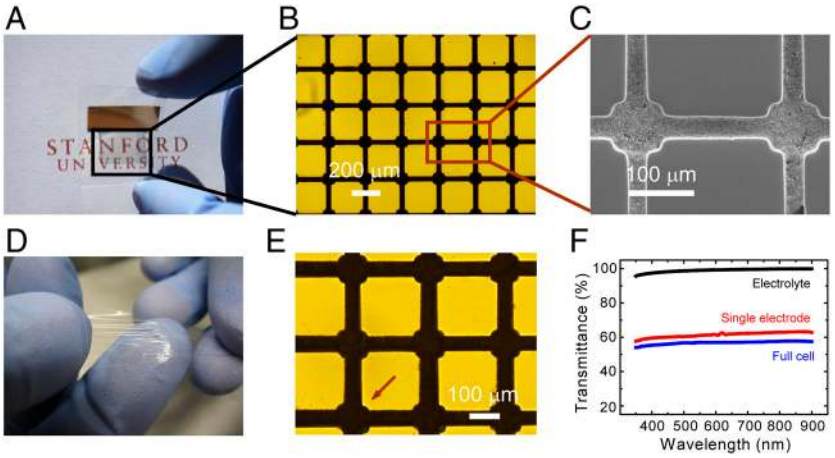

Fig. 2. (*A*) Photographic image of a transparent and flexible battery electrode. (*B* and *C*) Magnified optical image (*B*) and SEM image (*C*) of the battery electrode. Electrode materials are only confined inside the trenches. (*D*) Transparent, flexible, and stretchable gel electrolyte. (*E*) Optical microscopic image of a full battery with electrodes matched to each other. A small mismatch (*Bottom Left*) is marked by the red arrow. (*F*) The UV-VIS spectrum of gel electrolyte, a single electrode, and a full battery.

ergy at the same time. This is accomplished by matching the electrodes manually under a microscope, but can be achieved automatically in the future. Fig. 2*E* shows an optical image of an assembled transparent Li-ion battery with two electrodes and a gel electrolyte membrane in between. It is clear that the two electrodes align well with each other and only a small mismatch is observed at the bottom left corner.

Transparency Measurement. To quantitatively study the transparency of battery components and the full device, UV-visible (UV-VIS) spectroscopy is used to measure the transmittance of each component, as plotted in Fig. 2*F*. The gel electrolyte exhibits transmittance of about 99%, so its effect on the transparency of the full battery is negligible. A single electrode without packaging showed a transmittance of 62% in the visible and near infrared, which is 3% lower than the theoretical value based on the area of battery materials in the design. The difference may originate from the coverage area of the battery material, but could also occur because the UV-VIS spectrum only measures the direct transmittance, but not the diffuse transmittance. The full cell with packaging exhibits a transmittance of 57%. The 5% difference in transmittance between a single electrode and a full cell is likely a result of the small mismatch (3–5 μm) between the two electrodes, which is consistent with observations from optical microscopy images (Fig. 2*E*), or a small amount of absorption from the packaging. Nevertheless, the transmittance of the full cell is much higher than two electrodes randomly stacked ($0.65^2 \sim 42\%$). When more electrodes are stacked together, the difference will be even more significant. For example, a device with three full cells in series will exhibit a transparency less than 10% if they are randomly oriented. In contrast, well-aligned cells show transparency similar to an individual electrode (approximately 60%).

Electrochemical Characterizations. Before investigating the performance of the transparent battery, the electrochemical behavior of each component was examined first. PDMS and gold are not used in traditional batteries. PDMS has been previously reported as a component in a copolymer electrolyte (27). Gold is inert in the range of 1.0–4.4 V versus Li/Li^+ (28, 29), in which the operating potential range of the chosen cathode (3.5–4.25 V versus Li/Li^+ for $LiMn_2O_4$) and anode (1.3–1.8 V Li/Li^+ for $Li_4Ti_5O_{12}$) lie. To further test the stability of the gold film on PDMS, cyclic voltammetry was performed, showing little reaction with lithium in the potential window (Fig. S4). A small anodic peak is observed at 2.1 V, but it disappears after several scans. This indicates that the initial Coulomb efficiency might be slightly low at the anode side ($Li_4Ti_5O_{12}$). However, the current density is less than 10 $\mu A/cm^2$ at 2 mV/s, which is much less than the current used in charging/discharging batteries (100 $\mu A/cm^2$). Furthermore, because the peak diminishes quickly upon scanning and does not remain within the potential window for the full cell, this side reaction has little effect on battery performance after the first cycle. This argument is also supported by full cell cycling data discussed later in this paper.

Fig. 3*A* exhibits the typical voltage profiles of $Li_4Ti_5O_{12}$ nanopowder and $LiMn_2O_4$ nanorods, respectively. The profiles are similar to those observed in conventional battery electrode (24, 30), and no significant overpotential is observed. To quantitatively understand how the grid design affects the voltage profile, we measured the resistance of the transparent electrodes. The sheet resistance is approximately 60 Ω/sq for both electrodes, suggesting an additional overpotential of only 3 mV in half cells at 100 $\mu A/cm^2$. The electrode is also flexible. Even after repeatedly bending down to a radius of 2 cm 100 times, the sheet resistance is still less than 100 Ω/sq. After bending, only a slightly higher overpotential is observed and the corresponding capacity is less than 5% lower than before bending (Fig. 3*A*, dashed line). Resistances of the electrode bent to different radii are measured and no dramatic change is observed at radii above 1 cm (Fig. S5). We attribute the good flexibility of transparent electrodes to two reasons: (*i*) the flexibility of PDMS and (*ii*) conductive carbon black can bridge cracked Au electrode pieces. The cycling performance of these transparent electrodes is shown in Fig. 3*B*. The $LiMn_2O_4$ nanorod and $Li_4Ti_5O_{12}$ nanopowder electrodes showed initial discharge capacities of 97 mAh/g and 142 mAh/g and capacity retentions of 87% and 93% after 40 cycles at 100 $\mu A/cm^2$, respectively. To derive the specific capacity, the mass loading is calculated based on the tapping density and the thickness of the electrode film. The tapping density is estimated from electrode films with the same composition coated by doctor blading with the same composition, which is 1.1 g/cm^3 for $LiMn_2O_4$ and 1.2 g/cm^3 for $Li_4Ti_5O_{12}$ electrodes, respectively. As a result, the estimated mass loading is 1.8 mg/cm^2 for $LiMn_2O_4$ and 1.9 mg/cm^2 for $Li_4Ti_5O_{12}$, which leads to specific capacity consistent with previous reports (20, 24, 30). The Coulomb efficiency is above 97% for both electrodes. Passivation of PDMS with transparent materials (e.g., polymer or oxides) could further improve the Coulomb efficiency. Impedance measurements show that the transparent gel electrolyte has an ionic conductivity of 2×10^{-3} S/cm, which satisfies the requirement for commercial batteries (Fig. S6).

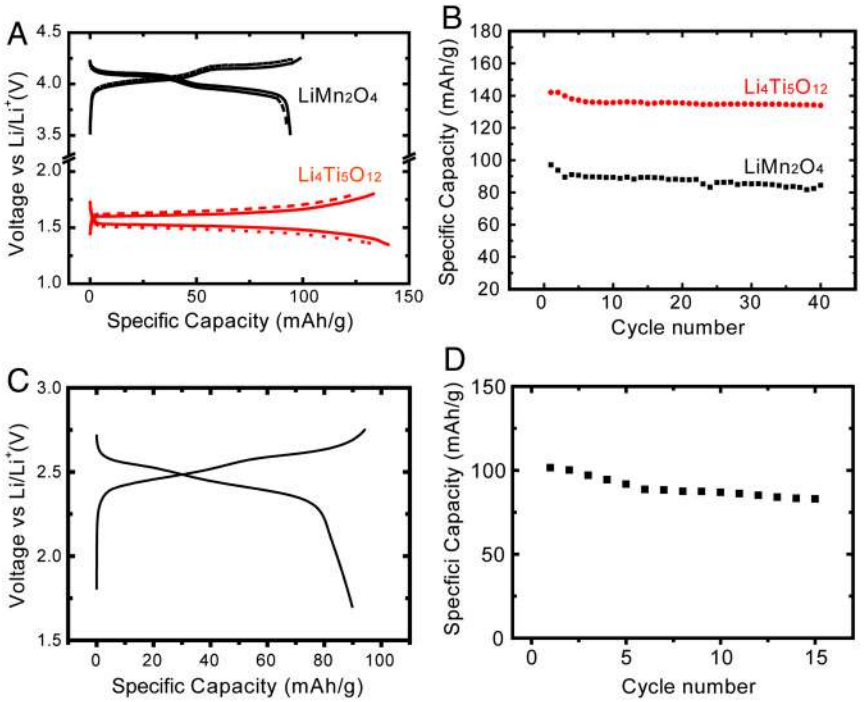

Fig. 3. (*A* and *B*) The voltage profile (*A*) and the cycling performance (*B*) of a transparent cathode ($LiMn_2O_4$ nanorods) and anode ($Li_4Ti_5O_{12}$ nanoparticles) in half cells with lithium as the counter electrode. Solid and dashed lines represent as-fabricated electrodes and electrodes after bending to 2 cm in radius 100 times, respectively. The applied current is 100 μA/cm^2. The transparency of electrodes is about 65%. (*C* and *D*) The voltage profile (*C*) and the cycling performance (*D*) of a transparent $LiMn_2O_4/Li_4Ti_5O_{12}$ full cell with transparency of 60%. The current is 100 μA/cm^2.

The transparent full cell is fabricated by sealing $LiMn_2O_4$ electrode/gel electrolyte/$Li_4Ti_5O_{12}$ electrode inside a transparent plastic bag, which has the same configuration as a pouch cell. Fig. 3 *C* and *D* shows the voltage profile and cycling performance, respectively. The average discharge voltage is 2.4 V, consistent with the difference between $LiMn_2O_4$ and $Li_4Ti_5O_{12}$. The initial discharge capacity is 100 mAh/g, and the capacity remains over 80 mAh/g after 15 cycles.

To demonstrate practical applications, the transparent full cell is used to repeatedly light a red light emitting diode (LED), as shown in Fig. 4*A*. The LED is placed behind a transparent battery and light shines through it. The energy density of this full cell is 50 Wh/L based on active electrode materials only and 10 Wh/L including all components.

In Situ Raman Study Based on Transparent Batteries. Besides applications in transparent electronics, the transparent battery is also a useful research tool for scientific studies. As the cell is transparent, electrode materials are visible. Consequently, optical methods, such as Raman spectroscopy and FTIR, could be applied to in situ studies of electrode materials. Furthermore, as the electrode is well patterned, it is possible to investigate of the effect of geometry on the charge/discharge of electrode materials. Fig. 4*B* shows in situ micro-Raman spectra collected in a transparent battery. In this case, the two electrodes are slightly mismatched so that the laser (Ar^+, 514 nm) illuminates on the $LiMn_2O_4$ electrode. Three spectra are collected upon charging, corresponding to $x = 1.0$, 0.5, and 0.2 in $Li_xMn_2O_4$. Two peaks at 498 and 717 cm^{-1} originate from PDMS and do not change in all three spectra. PDMS exhibits another small peak at 612 cm^{-1}, which is covered by the peak at 626 cm^{-1}, the A_{1g} mode in $LiMn_2O_4$ (31, 32). When x decreases to 0.5, this peak becomes lower and shifts to 620 cm^{-1}. After more lithium is extracted and x further decreases down to 0.2, a strong peak at 597 cm^{-1} is observed, corresponding to the A_{1g} mode in λ-MnO_2 (31, 32). The observation of the evolution of Raman peaks demonstrates

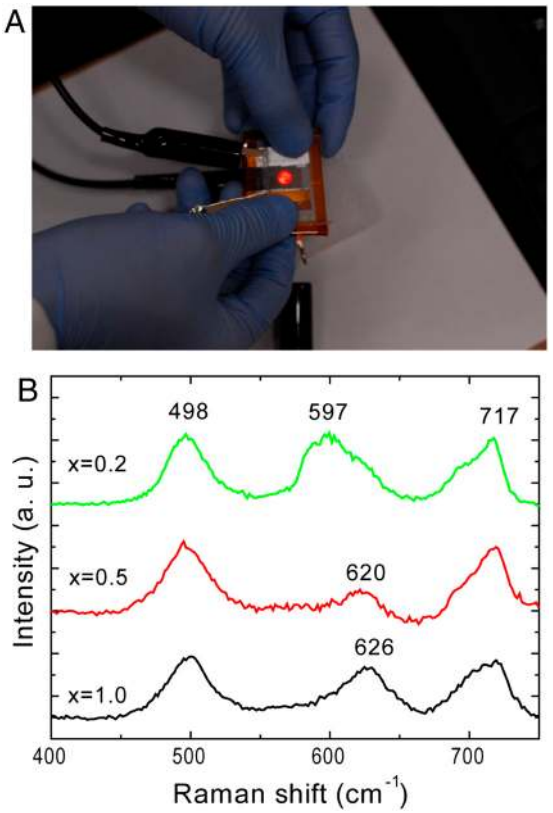

Fig. 4. (*A*) A transparent battery lighting a red LED. The cell is sealed with Kapton tape. The LED is placed behind the battery so that light shines through the transparent battery. (*B*) In situ Raman spectrum of $Li_xMn_2O_4$ nanorods at different charging states (x) measured in a transparent battery. The two peaks at 498 and 717 cm^{-1} belong to PDMS, whereas peaks at 625 and 597 cm^{-1} can be assigned to $LiMn_2O_4$ and λ-MnO_2, respectively.

the feasibility of using a transparent battery for an in situ optical spectroscopy study of fundamental electrochemical reactions.

Discussion

The theoretical energy density with packaging is 100 Wh/L, about one order of magnitude higher than the transparent battery demonstrated. The difference mainly comes from a thick PDMS substrate (approximately 100 μm) and thin electrode film (approximately 50 μm). With further optimization, including reducing the thickness of PDMS substrate, increasing the depth of the trenches and using materials with higher specific capacity and tapping density (e.g., $LiCoO_2$), we believe that the energy density could be increased to over 50 Wh/L.

Moreover, in some types of portable electronics and miniaturized devices, the footprint area is limited, but the restriction on device thickness is less stringent. As a result, the energy per area is more important than the energy per volume for certain applications (33, 34). Given the opportunity to stacking multiple cells in series, which increases the areal energy density without sacrificing the transparency, our unique electrode grid design is favorable to thin film designs and will result in practical transparent batteries.

In this paper, we have proposed and realized an approach to pattern battery electrodes at the micron scale to fabricate transparent batteries, which can function as the power supply in transparent electronics. As the feature size of the patterned electrode is less than the resolution of human eyes, the nontransparent electrode materials cannot be distinguished from the transparent PDMS substrate, resulting in a transparent electrode. The grid-like structure of the electrode is achieved through a unique method based on microfluidic techniques, which allows us to fabricate battery electrodes with a well-defined grid structure. Furthermore, by aligning multiple electrodes together, the transparency does not decrease, whereas the energy stored in the battery increases linearly with the number of electrodes. The as-fabricated devices show transparency of 78, 60, and 30% and corresponding energy density of 5, 10, and 20 Wh/L with packaging.

Materials and Methods

Materials. $LiMn_2O_4$ is synthesized by annealing a mixture of β-MnO_2 nanorods and lithium acetate (20), and $Li_4Ti_5O_{12}$ powders are from Hydro-Québec. To make gel electrolyte, 1 M $LiClO_4$ in EC/DEC and PVDF-HFP is first dissolved in tetrahydrofuran. After stirring, the clear solution is drop cast onto a glass slide and dried to remove tetrahydrofuran. The membrane is soaked in 1 M $LiClO_4$ in EC/DEC after drying.

Fabrication of Transparent Battery. PDMS substrate with grid trenches is fabricated by spin coating PDMS precursor (Sylgard 184) onto a silicon mold patterned by photolithography. The PDMS film is cured at 80 °C and peeled off from the mold. After 100 nm gold is evaporated onto PDMS as the current collector, the substrate surface is made hydrophilic by air plasma. Then the electrode material solution is filled in by a microfluidics-assisted method. The electrode material is composed of 90% active materials ($LiMn_2O_4$ or $Li_4Ti_5O_{12}$), 7% carbon black, and 3% aqueous binder (Pred materials). The concentration of solid materials in the solution is 18–20%.

To introduce the slurry solution to the predesigned trenches, a thin slide of PDMS is placed at one end of the electrode region to form an area of closed channels. Then the slurry solution is dropped onto one side of the channels. Because of the capillary force, the aqueous solution is sucked into channels under the blocking PDMS and then continues flowing in the channels not covered by PDMS. The flowing speed is about 1 cm/s. Then the solution is dried and the blocking PDMS piece is removed. Finally, a piece of Kapton tape is carefully pressed onto the PDMS substrate and extra gold film is peeled off.

To make a full cell, aluminum strip is wrapped onto the side of each electrode. Then, gel electrolyte is placed on the anode electrode first, and the transparent cathode is put on the anode under optical microscope at 20×. The full cell is sealed inside a highly transparent poly(vinyl chloride) (PVC) thermoplastic bag with metal current collector extending out. The cell configuration is very similar to a pouch cell except that all components are transparent.

Electrochemical Measurement. Half cell is made by sealing the electrode in transparent plastic bags in a glove box. Lithium foil is used as the counter electrode in half cells and the electrolyte is the transparent gel membrane. For full cell tests, the gel electrolyte membrane is sandwiched between two transparent electrodes. Then the full cell is packed in transparent plastic bags. Cyclic voltammetry is performed in a three-electrode configuration, where both counter and reference electrode are lithium. PVC sealing bags are used in all electrochemical tests.

Transmittance Test. UV-VIS spectroscopy is used to measure the transmittance of samples. A glass slide is used as the reference. For half cell and gel electrolyte, packaging is not included, whereas the transparency of full cell is measured with packaging.

ACKNOWLEDGMENTS. We thank Jianbin Wang and Yu Lin for helpful discussions. We acknowledge Wenshan Cai for drawings. We thank Sy Bohy for viscosity measurements. Karim Zaghib (Hydro-Québec, Varennes, Canada) is acknowledged for providing $Li_4Ti_5O_{12}$ samples. Y.Y. acknowledges support from a Stanford Graduate Fellowship. S.J. acknowledges support from the Korea Foundation for Advanced Studies. S.W.L. acknowledges support from King Abdullah University of Science and Technology (KAUST). The work is supported by KAUST under Award KUS-I1-001-12.

1. Sanghyun J, et al. (2007) Fabrication of fully transparent nanowire transistors for transparent and flexible electronics. *Nat Nanotechnol* 2:378–384.
2. Yu GH, Cao AY, Lieber CM (2007) Large-area blown bubble films of aligned nanowires and carbon nanotubes. *Nat Nanotechnol* 2:372–377.
3. Cao Q, et al. (2006) Highly bendable, transparent thin-film transistors that use carbon-nanotube-based conductors and semiconductors with elastomeric dielectrics. *Adv Mater* 18:304–309.
4. Lian W, et al. (2006) High-performance transparent inorganic-organic hybrid thin-film n-type transistors. *Nat Mater* 5:893–900.
5. Artukovic E, Kaempgen M, Hecht DS, Roth S, GrUner G (2005) Transparent and flexible carbon nanotube transistors. *Nano Lett* 5:757–760.
6. Nomura K, et al. (2003) Thin-film transistor fabricated in single-crystalline transparent oxide semiconductor. *Science* 300:1269–1272.
7. Wu ZC, et al. (2004) Transparent, conductive carbon nanotube films. *Science* 305:1273–1276.
8. Park SI, et al. (2009) Printed assemblies of inorganic light-emitting diodes for deformable and semitransparent displays. *Science* 325:977–981.
9. Ju S, et al. (2008) Transparent active matrix organic light-emitting diode displays driven by nanowire transistor circuitry. *Nano Lett* 8:997–1004.
10. Gorrn P, et al. (2006) Towards see-through displays: Fully transparent thin-film transistors driving transparent organic light-emitting diodes. *Adv Mater* 18:738–741.
11. Bae S, et al. (2010) Roll-to-roll production of 30-inch graphene films for transparent electrodes. *Nat Nanotechnol* 5:574–578.
12. Lee JY, Connor ST, Cui Y, Peumans P Semitransparent organic photovoltaic cells with laminated top electrode. *Nano Lett* 10:1276–1279.
13. Yoon J, et al. (2008) Ultrathin silicon solar microcells for semitransparent, mechanically flexible and microconcentrator module designs. *Nat Mater* 7:907–915.
14. Huang JS, Li G, Yang Y (2008) A semi-transparent plastic solar cell fabricated by a lamination process. *Adv Mater* 20:415–419.
15. Tarascon JM, Armand M (2001) Issues and challenges facing rechargeable lithium batteries. *Nature* 414:359–367.
16. Hong JK, Lee JH, Oh SM (2002) Effect of carbon additive on electrochemical performance of LiCoO2 composite cathodes. *J Power Sources* 111:90–96.
17. Ho WH, Li CF, Liu HC, Yen SK (2008) Electrochemical performance of In_2O_3 thin film electrode in lithium cell. *J Power Sources* 175:897–902.
18. Chen PC, Shen G, Sukcharoenchoke S, Zhou C (2009) Flexible and transparent supercapacitor based on In_2O_3 nanowire/carbon nanotube heterogeneous films. *Appl Phys Lett* 94:043113.
19. Martin F, et al. (2010) High-energy, efficient and transparent electrode for lithium batteries. *J Mater Chem* 20:2847–2852.
20. Yang Y, et al. (2009) Single nanorod devices for battery diagnostics: A case study on $LiMn_2O_4$. *Nano Lett* 9:4109–4114.
21. Kang B, Ceder G (2009) Battery materials for ultrafast charging and discharging. *Nature* 458:190–193.
22. Gates B, Qin D, Xia YN (1999) Assembly of nanoparticles into opaline structures over large areas. *Adv Mater* 11:466–469.
23. Kim E, Xia YN, Whitesides GM (1996) Two- and three-dimensional crystallization of polymeric microspheres by micromolding in capillaries. *Adv Mater* 8:245–247.
24. Kim DK, et al. (2008) Spinel LiMn2O4 nanorods as lithium ion battery cathodes. *Nano Lett* 8:3948–3952.
25. Xue MQ, et al. (2009) Transfer printing of metal nanoparticles with controllable dimensions, placement, and reproducible surface-enhanced raman scattering effects. *Langmuir* 25:4347–4351.
26. Arora P, Zhang ZM (2004) Battery separators. *Chem Rev* 104:4419–4462.
27. Bouridah A, Dalard F, Deroo D, Cheradame H, Lenest JF (1985) Poly(dimethylsiloxane)-poly(ethylene oxide) based polyurethane networks used as electrolytes in lithium electrochemical solid-state batteries. *Solid State Ionics* 15:233–240.
28. Mui SC, et al. (2002) Block copolymer-templated nanocomposite electrodes for rechargeable lithium batteries. *J Electrochem Soc* 149:A1610–A1615.

29. Lim MR, Cho WI, Kim KB (2001) Preparation and characterization of gold-codeposited $Limn_2O_4$ electrodes. *J Power Sources* 92:168–176.
30. Zaghib K, Simoneau M, Armand M, Gauthier M (1999) Electrochemical study of $Li_4Ti_5O_{12}$ as negative electrode for Li-ion polymer rechargeable batteries. *J Power Sources* 81–82:300–305.
31. Ammundsen B, Burns GR, Islam MS, Kanoh H, Roziere J (1999) Lattice dynamics and vibrational spectra of lithium manganese oxides: A computer simulation and spectroscopic study. *J Phys Chem B* 103:5175–5180.
32. Huang WW, Frech R (1999) In situ Raman spectroscopic studies of electrochemical intercalation in $Li_xMn_2O_4$-based cathodes. *J Power Sources* 81–82:616–620.
33. Long JW, Dunn B, Rolison DR, White HS (2004) Three-dimensional battery architectures. *Chem Rev* 104:4463–4492.
34. Baggetto L, Roozeboom F, Niessen RAH, Notten PHL (2008) On the route toward 3D-integrated all-solid-state micro-batteries. *Solid State Technol* 51:30–35.